Nuclear Inst. and Methods in Physics Research, A 989 (2021) 164956

Contents lists available at ScienceDirect

Nuclear Inst. and Methods in Physics Research, A

journal homepage: www.elsevier.com/locate/nima

Beam test results of NDL Low Gain Avalanche Detectors (LGAD)

S. Xiao [a,b], S. Alderweireldt [c], S. Ali [d], C. Allaire [c], C. Agapopoulou [e], N. Atanov [f], M.K. Ayoub [a], G. Barone [g], D. Benchekroun [h], A. Buzatu [d], D. Caforio [i], L. Castillo García [j], Y. Chan [k], H. Chen [l], V. Cindro [m], L. Ciucu [d], J. Barreiro Guimarães da Costa [a], H. Cui [a,b], F. Davó Miralles [j], Y. Davydov [f], G. d'Amen [g], C. de la Taille [n], R. Kiuchi [a], Y. Fan [a], A. Falou [e], A.S.C. Ferreira [c], M. Garau [o], J. Ge [l], A. Ghosh [p], G. Giacomini [g], E.L. Gkougkousis [j], C. Grieco [j], S. Guindon [c], D. Han [q], S. Han [a,b], M. Holmberg [r], A. Howard [m], Y. Huang [a], Y. Huang [k], M. Jing [a,b], Y. Khoulaki [h], G. Kramberger [m], E. Kuwertz [c], H. Lefebvre [s], M. Leite [t], A. Leopold [u], C. Li [l], Q. Li [l], H. Liang [l], Z. Liang [a], B. Liu [a], J. Liu [a], A. Luthfi [c], F. Lyu [a], S. Malyukov [f], I. Mandić [m], L. Masetti [v], M. Mikuž [m], I. Nikolic [u], L. Polidori [v], R. Polifka [w], O. Posopkina [c], B. Qi [a,b], K. Ran [a,b], B.J.G. Reynolds [y], C. Rizzi [c], M. Robles Manzano [v], E. Rossi [g], A. Rummler [c], S. Sacerdoti [e], G.T. Saito [t], N. Seguin-Moreau [n], L. Serin [e], L. Shan [a], L. Shi [a], X. Shi [a,*], N.F. Sjostrom [r], A. Soares Canas Ferreira [c], J. Soengen [v], H. Stenzel [i], A.J. Szadaj [r], Y. Tan [a,b], S. Terzo [j], J.O. Thomas [x], E. Tolley [y], A. Tricoli [g], S. Trincaz-Duvoid [u], R. Wang [v], S.M. Wang [d], W. Wang [z], W. Wang [l], K. Wu [a,b], T. Yang [a,b], Y. Yang [a], C. Yu [a,b], X. Zhang [q], L. Zhao [l], M. Zhao [a], Z. Zhao [l], X. Zheng [l], X. Zhuang [a]

[a] Institute of High Energy Physics, Chinese Academy of Sciences, 19B Yuquan Road, Shijingshan District, Beijing 100049, China
[b] University of Chinese Academy of Sciences, 19A Yuquan Road, Shijingshan District, Beijing 100049, China
[c] CERN, Esplanade des Particules 1, 1211 Geneva 23, Switzerland
[d] Academia Sinica, Nangang District, Taipei, Taiwan
[e] LAL, IN2P3-CNRS and Université Paris Sud, 91898 Orsay Cedex, France
[f] Joint Institute for Nuclear Research, Joliot-Curie street 6, Dubna, 141980, Russia
[g] Brookhaven National Laboratory (BNL), Upton, NY 11973, USA
[h] University of Hassan II Casablanca, Casablanca, Morocco
[i] Justus Liebig University Giessen, Ludwigstrasse 23, Giessen, Hesse 35390, Germany
[j] Institut de Física d'Altes Energies (IFAE), Carrer Can Magrans s/n, Edifici Cn, Universitat Autónoma de Barcelona (UAB), E-08193 Bellaterra, Barcelona, Spain
[k] National Tsing Hua University, Kuang-Fu Road, Hsinchu, Taiwan
[l] Department of Modern Physics and State Key Laboratory of Particle Detection and Electronics, University of Science and Technology of China, Hefei 230026, China
[m] Jozef Stefan Institut (JSI), Jamova 39, SI-1000, Ljubljana, Slovenia
[n] Omega Group, Brookhaven National Laboratory, BNL, USA
[o] University of Cagliari, Via Universitá 40, Cagliari, Sardinia 09124, USA
[p] University of Iowa, 116 Calvin Hall, Iowa City, IA 52242, USA
[q] Novel Device Laboratory, Beijing Normal University, No. 19, Xinjiekouwai Street, Haidian District, Beiing 100875, China
[r] KTH Royal Institute of Technology in Stockholm, Kungliga Tekniska Högskolan, SE-100 44, Sweden
[s] Royal Holloway University Of London, University Of London, Egham TW20 0EX, UK
[t] Instituto de Física - Universidade de São Paulo (USP), R. do Matão, 1371, Cidade Universitária, São Paulo 05508-090, Brazil
[u] LPNHE, Sorbonne Université, Université de Paris, CNRS/IN2P3, Paris, France
[v] University of Mainz, Saarstr. 21, Mainz, Rhineland-Palatinate 55122, Germany
[w] Charles University In Prague, Ovocný trh 3-5, Prague 116 36, Czech Republic
[x] Southern Methodist University, 6425 Boaz Ln, Dallas, TX 75205, USA
[y] Ohio State University, Columbus, OH, USA
[z] Nanjing University, 22 Hankou Road, Nanjing, Jiangsu 210093, China

* Corresponding author at: Institute of High Energy Physics, Chinese Academy of Sciences, 19B Yuquan Road, Shijingshan District, Beijing 100049, China.
E-mail address: shixin@ihep.ac.cn (X. Shi).

https://doi.org/10.1016/j.nima.2020.164956
Received 16 March 2020; Received in revised form 2 December 2020; Accepted 5 December 2020
Available online 15 December 2020

ARTICLE INFO

Keywords:
LGAD
Time resolution
Electron beam
CFD

ABSTRACT

A High-Granularity Timing Detector (HGTD) is proposed based on the Low-Gain Avalanche Detector (LGAD) for the ATLAS experiment to satisfy the time resolution requirement for the up-coming High Luminosity at LHC (HL-LHC). We report on beam test results for two proto-types LGADs (BV60 and BV170) developed for the HGTD. Such modules were manufactured by the Institute of High Energy Physics (IHEP) of Chinese Academy of Sciences (CAS) collaborated with Novel Device Laboratory (NDL) of the Beijing Normal University. The beam tests were performed with 5 GeV electron beam at DESY. The timing performance of the LGADs was compared to a trigger counter consisting of a quartz bar coupled to a SiPM readout while extracting reference SiPM by fitting with a Gaussian function. The time resolution was obtained as 41 ps and 63 ps for the BV60 and the BV170, respectively.

1. Introduction

Low-gain avalanche detectors (LGADs) are suggested for applications at the HL-LHC where the pile-up of multiple proton–proton collisions are estimated for over 200 interaction vertices. To alleviate the high luminosity induced pile-up, the high-granularity timing detector (HGTD) is proposed at ATLAS to present the timing information for the particle tracks and distinguish the originated interaction vertices. The target average time resolution of the tracking detector is 30 ps. The low-gain avalanche detector is selected as the key sensor technology for the HGTD [1–3].

The LGADs are n-on-p silicon detectors containing an additional highly-doped p-layer under the n-p junction as shown in Fig. 1(a) [2]. It creates a high field resulting in internal amplification. More electron and hole pairs are generated by crossing the initial carriers through the amplification layer. The LGADs have been developed by the CERN-RD50 [4] with detectors fabricated by the CNM Barcelona [2], Hamamatsu Photonics [5] and FBK Italy [6]. Recently, the Institute of High Energy Physics (IHEP) cooperated with Novel Device Laboratory (NDL) of the Beijing Normal University also combined the task force to build LGADs for the HGTD project.

Two types of NDL LGADs are made with various volume resistivity for silicon epitaxial layer with 300 Ω·cm for BV60 and 100 Ω·cm for BV170, respectively. The detector layout is shown in Fig. 1(b). It contains 2 × 2 pads implemented in an area of 3.2 × 3.2 mm^2 surrounded by six guard rings. The size of each pad is 1.0 × 1.0 mm^2 covered with silicon oxide and aluminum lines. The wafer thickness is 300 μm and the thickness of active epitaxial layer is 33 μm. The beam tests were conducted at DESY to investigate the timing performance of these LGADs. The signal amplitude and the electronic noise were the key factors to time resolution, which were compared to the results conducted with a pico-second laser pulse [7] while obtaining the time resolution of 10 ps.

2. Properties of NDL detectors

The two types of NDL LGADs were measured for the Current–Voltage (I–V) and Capacitance–Voltage (C–V) characteristics on a probe station at room temperature. The results are plotted in Fig. 2. The curvatures of these plots are used to extract the transition voltage values for full breakdown and depletion which are listed in Table 1. The "foot voltage" is also listed, which is the value for the gain layer being depleted. The foot voltages of the BV60 and the BV170 are similar indicating the doping concentration of gain layers implemented at the same level. The different depletion voltages are resultant from various bulk resistivity in the epitaxial layers.

The time resolution of LGADs can be explained with contributions of the following [1]:

$$\sigma^2 = \sigma^2_{Signal\ distortion} + \sigma^2_{Time\ walk} + \sigma^2_{Landau\ noise} + \sigma^2_{Digitization\ noise} + \sigma^2_{Jitter} \quad (1)$$

where $\sigma_{Signal\ distortion}$ term represents the smearing factor caused by the non-uniform drift velocity and weighting field according to the Ramo–Shockley's theorem [1]. The $\sigma_{Time\ walk}$ term is resultant from the shift of arrival time among pulses with various signal amplitudes. The time walk effect is minimized using the Constant Fraction Discriminator (CFD) method. Since the detector has a lower thickness compared to the pad size, the contribution from time walk to Landau can be ignored. The $\sigma_{Landau\ noise}$ is caused by the non-uniform energy deposition of the traversing beam particles. It is the main factor in the resolution, which is estimated with the results from previous laser measurements. The $\sigma_{Digitization\ noise}$ is attributed to the noise of the digital oscilloscope for signal waveform measurements. The σ_{Jitter} accounts for the electronic noise of the readout. It is approximated as $\sigma_{Jitter} = N/(dV/dt) \approx t_{rise}/(S/N)$ [1], with a linear dependence on the increasing time of the signal pulse (t_{rise}) and is inversely proportional to the signal to noise ratio (S/N).

3. Experimental set-up

The NDL LGADs were tested at DESY with 5 GeV electrons in a test beam facility [8]. Each LGAD test sample was wire bonded on a ~ 10 × 10 cm^2 read-out circuit board as shown in Fig. 3. The circuit board established by the UCSC group [9] consists of a silicon-germanium bipolar transistor coupled to a 2 GHz amplifier. The test beam facility is equipped with the EUDET-type beam telescope [10] measuring the electron tracks traversing the "devices under test" (DUTs) as shown in Fig. 4. The beam telescope includes six-pixel detector planes using multi-input multi-output silicon accelerator (MIMOSA) sensors. The Trigger Logic Unit (TLU) possesses an FE-I4 based pixel sensor module [11] in coincidence the MIMOSA outputs. An oscilloscope (10 GS/s sample rate) triggered by the TLU is used to measure the waveforms of LGAD signals. The MIMOSA readouts for each trigger are recorded by the data acquisition system instrumented in a PXIe crate. As a timing reference, a fast Cherenkov counter made of quartz bar is situated in the beam line. The timing performance of the LGADs is assessed with three various bias voltages during the beam tests. The corresponding depletion and breakdown voltages are different, for which the results are compared to optimize the values selected in normal operation.

4. Results

4.1. Data analysis

The LGADs signal waveforms as shown in Fig. 5 recorded during the beam tests with 5 GeV electrons were analyzed for the increasing time and amplitude. The analysis framework of PyAna is used for event reconstruction.

The oscilloscope records all the waveforms created during the run period including the time and amplitude information of DUTs. The noise is defined as the root mean square value of the amplitude distribution of the first point in each waveform. The signal charge is determined by the product of current and time as $Q = \sum_i^n (I_i \times \Delta t)$ where Δt is a

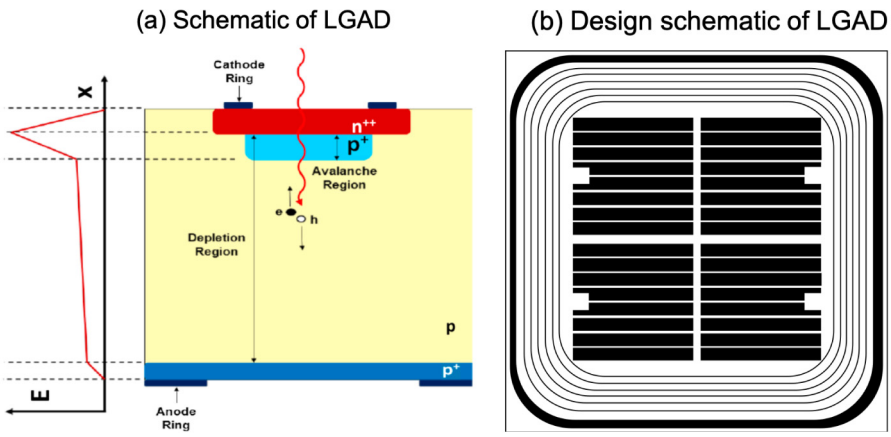

Fig. 1. (a) The schematic of an n-on-p LGAD [2]. An additional highly-doped p-layer is under the n-p junction where there is a high electric field. (b) The design schematic of the NDL LGAD sensor. 2 × 2 pads are made with six guard rings. The whole size of the detector is 3.2×3.2 mm^2 while the size of each pad is 1.0×1.0 mm^2 covered with black silicon oxide and white aluminum lines.

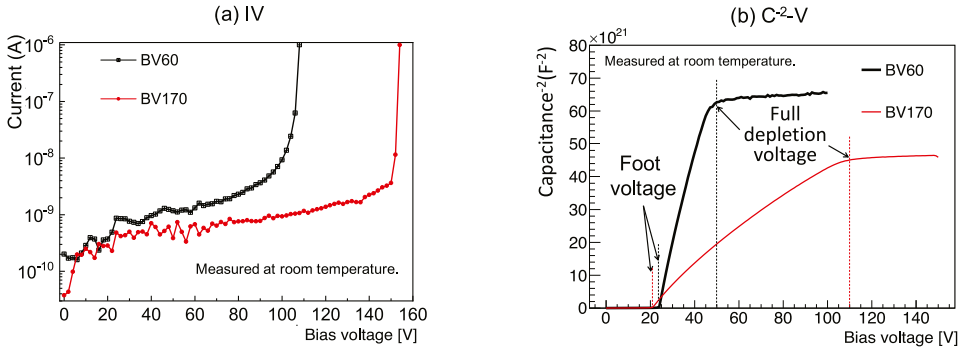

Fig. 2. The IV curve of NDL LGADs and C^{-2} vs. bias voltage for NDL LGADs [7].

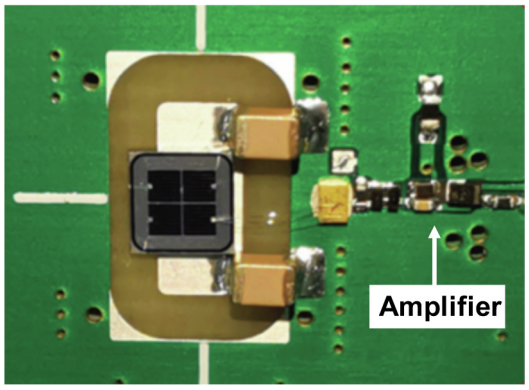

Fig. 3. Photo of the NDL LGAD wire-bonded to UCSC read-out board with trans-impedance first stage amplifier [7,12]. A 5 GHz silicon-germanium bipolar transistor is coupled to a 2 GHz amplifier.

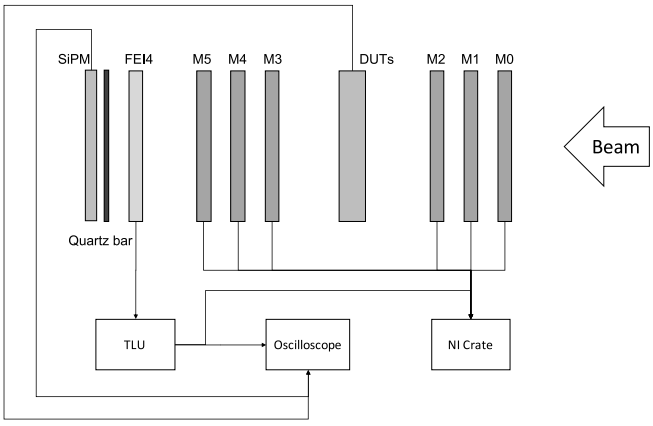

Fig. 4. The test beam passes through MIMOSA sensors (M0 to M5), LGADs under test (DUTs), FE-I4, and the reference SiPM. MIMOSA planes are used to offer the information for tracking while FE-I4 and TLU are utilized for triggering. The data from the LGADs and SiPM are collected by the oscilloscope while saving the beam telescope and FE-I4 data in the NI crate.

constant time interval extracted from sampling rate. The CFD method is applied to locate the timing point at the selected fraction of the signal waveform. The time resolution of the LGADs is assessed for the CFD values of 20, 50 and 70.

The LGAD signals are the ionization charges collected from beam electrons traversing through the silicon wafer. The pulse height distribution follows Landau distribution. The pulse height and signal charges are fitted with a Landau function convoluted with a Gaussian function. A Gaussian function is utilized to describe the noise distribution. The S/N is calculated using amplitude over the noise. S denotes the Landau most probable value and N is the Gaussian width. The waveforms of the LGADs gathered in the beam tests are examined for the signal amplitude, noise, their ratio (S/N) and the integrated total charge are plotted in Fig. 6. The results indicate that the higher bias voltage to LGADs leads to the higher pulse height and more signal charges. It is found that the noise is independent of the bias voltage as a result of the low leakage current compared to the electronic noise. The BV60 collects more charges than 4 fC which is required by ATLAS HGTD TDR [13],

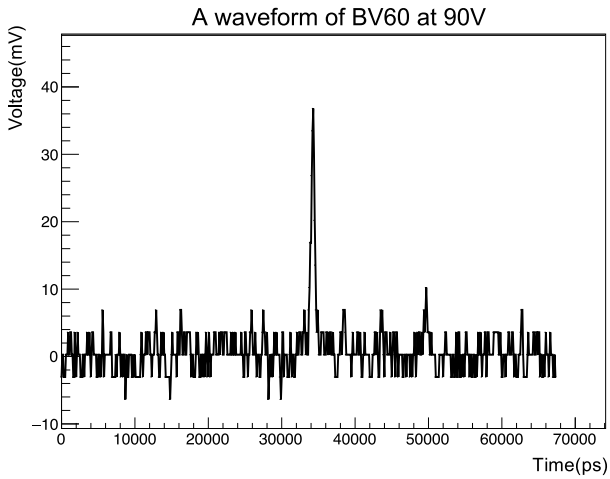

Fig. 5. A typical LGAD waveform recorded in beam tests through Teledyne LeCroy WaveRunner 8104 at 10 GS/s.

Table 1
The foot voltages, depletion voltages and breakdown voltages of BV60 and BV170 extracted from Fig. 2.

Items	BV60 [V]	BV170 [V]
Foot voltage	24	21
Depletion voltage	50	110
Breakdown voltage	110	160

however, the charges BV170 collects is less than 4 fC due to its low volume resistivity in epitaxial layer.

4.2. Time resolution

The beam test setup includes a quartz bar where the Cherenkov light generated by traversing electrons is collected by a SiPM readout, which is taken as the reference detector to assess the time resolutions of LGADs. It detects the Cherenkov photons generated by electrons in quartz, $3 \times 3 \times 10$ mm^3, 6 side-polished. Then, the signals from SiPM are boosted by an amplifier with a gain of 10. The signal rise times of the BV60, BV170, and the reference SiPM readout are analyzed using the CFD technique applying three different thresholds. Each of the time resolutions of BV60, BV170, and SiPM can be combined into three various pairs. The time difference of each pair with different CFD values can be explained with a Gaussian function [9]. The sigma of the fitted Gaussian function is the time resolution for each pair as shown in Fig. 7. Assuming that there is no correlation in each pair, the time resolutions of reference SiPM and LGADs can be calculated with the time resolutions of each pair and the error propagation. To illustrate the calculation, the pair of BV60 and SiPM is taken as an example. The time resolution of BV60 can be determined as

$$\sigma_{BV60} = \sqrt{\sigma^2_{(BV60,SiPM)} - \sigma^2_{SiPM}} \quad (2)$$

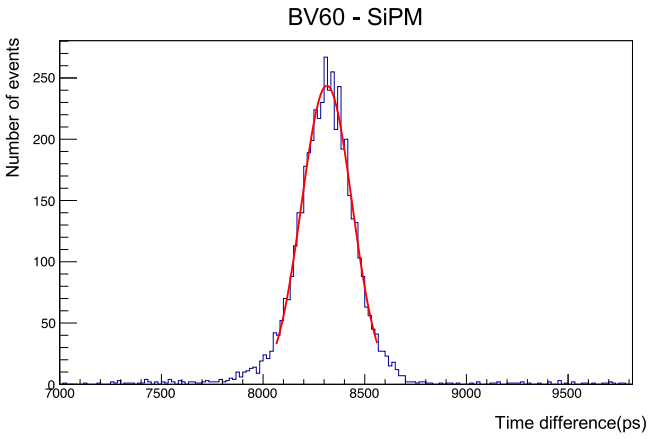

Fig. 7. Gaussian function is utilized to fit the time difference of reference SiPM and BV60 at 50 V (CFD20). σ of this Gaussian distribution is taken as the time resolution of this system.

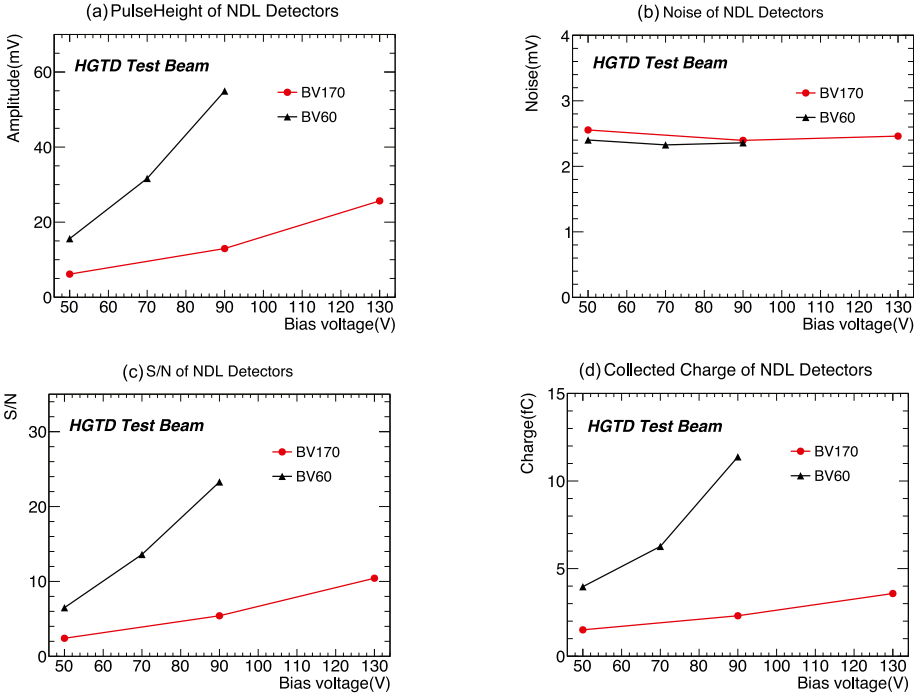

Fig. 6. The performance of NDL LGADs BV60 and BV170. (a) Amplitude increases by increasing the voltage. (b) Noise distribution is voltage independent. (c) S/N distribution for BV60 and BV170, determined by amplitude over noise. (d) Collected charge. BV60 collects more charges than 4 fC.

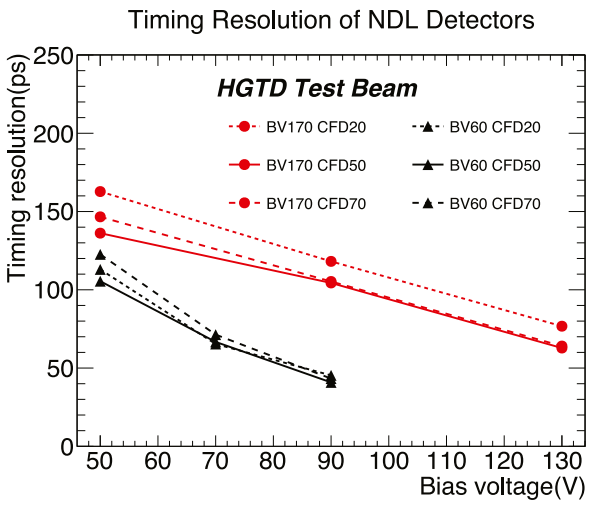

Fig. 8. Time resolution for BV60 and BV170 as function of bias voltage. The time resolutions of these two detectors are getting better as bias voltage goes up. The CFD50 leads to smaller time resolutions than CFD20 and CFD70.

with uncertainty

$$\delta_{BV60} = \sqrt{\frac{[\sigma_{(BV60,SiPM)}\delta_{(BV60,SiPM)}]^2 + (\sigma_{SiPM}\delta_{SiPM})^2}{\sigma^2_{(BV60,SiPM)} - \sigma^2_{SiPM}}} \quad (3)$$

The reference Quartz counter with SiPM readout was utilized in several beam tests at CERN and DESY. Long-term exposure to beam particles results in a degraded performance as 70 ± 1 ps (statistical uncertainty only) at 26.5 V. Shown in Fig. 8 are the distributions obtained for the time resolutions of BV60 and BV170. The signal rise times decrease by the higher bias voltage. The differences with different CFD values are also plotted. CFD at 50 leads to better time resolutions than CFD 20 and 70. The best time resolution obtained with BV60 is 41 ± 1ps at 90 V, and BV170 is 63 ± 1ps at 130 V (statistical uncertainties only), respectively.

5. Conclusion

The beam test was conducted on two types of NDL LGADs BV60 and BV170. BV60 gathered more charges than 4 fC to fulfill the requirement of ATLAS HGTD. However, the charges collected by BV170 are less than 4 fC due to its low epitaxial volume resistivity. With a CFD at 50, the best time resolutions of BV60 and BV170 are 41 ps and 63 ps, respectively. For further development of NDL LGADs, the thickness of the epitaxial layer is extended to 50 μm as the baseline of HGTD.

Declaration of competing interest

The authors declare that they have no known competing financial interests or personal relationships that could have appeared to influence the work reported in this paper.

Acknowledgments

The measurements leading to these results have been performed at the beam test Facility at DESY Hamburg (Germany), a member of the Helmholtz Association (HGF). Thanks to Beijing Normal University for the detector production, and DESY for the beam test setup and shifts. Thanks all colleagues involved in these processes. This work was supported by the National Natural Science Foundation of China (No. 11961141014), the State Key Laboratory of Particle Detection and Electronics (SKLPDE-ZZ-202001), and the Hundred Talent Program of the Chinese Academy of Sciences (Y6291150K2).

References

[1] H.F.-W. Sadrozinski, et al., 4D tracking with ultra-fast silicon detectors, Rep. Progr. Phys. 81 (2018) 026101.
[2] G. Pellegrini, et al., Technology developments and first measurements of Low Gain Avalanche Detectors (LGAD) for high energy physics applications, Nucl. Instrum. Methods Phys. Res. A 765 (2016) 12–16.
[3] G. Giacomini, et al., Development of a technology for the fabrication of Low-Gain Avalanche Detectors at BNL, Nucl. Instrum. Methods Phys. Res. A 934 (2019) 52–57.
[4] https://rd50.web.cern.ch/rd50.
[5] G. Kramberger, et al., Radiation hardness of thin Low Gain Avalanche Detectors, Nucl. Instrum. Methods Phys. Res. A 891 (2018) 68–77.
[6] M. Ferrero, et al., Radiation resistant LGAD design, Nucl. Instrum. Methods Phys. Res. A 919 (2019) 16–26.
[7] Y. Yang, et al., Charaterization of the first prototype NDL LGAD sensor, arXiv:1912.13211.
[8] R. Diener, et al., The DESY II beam test facility, Nucl. Instrum. Methods Phys. Res. A 922 (2019) 265–286.
[9] N. Cartiglia, et al., Beam test results of a 16 ps timing system based on ultra-fast silicon detectors, Nucl. Instrum. Methods Phys. Res. A 850 (2017) 83–88.
[10] H. Jansen, et al., Performance of the EUDET-type beam telescopes, arXiv:1603.09669v2.
[11] U. Koetz, et al., User Manual: ATLAS FE-I4A Pixel Module as a Trigger Plane for the Beam Telescope, DESY, 2013, https://telescopes.desy.de/Main_Page.
[12] https://twiki.cern.ch/twiki/pub/Main/UcscSingleChannel/proto_beam_test_board_V1.1C.pdf.
[13] ATLAS Collaboration, Technical Design Report: A High-Granularity Timing Detector for the ATLAS Phase-II Upgrade, CERN, 2020, https://cds.cern.ch/record/2719855.